Journal of Solid Mechanics Vol. 2, No. 1 (2010) pp. 1-18

Multiscale Analysis of Transverse Cracking in Cross-Ply Laminated Beams Using the Layerwise Theory

Wook Jin Na, J.N. Reddy*

Department of Mechanical Engineering, Texas A&M University, College Station, TX 77840, USA

Received 25 December 2009; accepted 23 January 2010

ABSTRACT

A finite element model based on the layerwise theory is developed for the analysis of transverse cracking in cross-ply laminated beams. The numerical model is developed using the layerwise theory of Reddy, and the von Kármán type nonlinear strain field is adopted to accommodate the moderately large rotations of the beam. The finite element beam model is verified by comparing the present numerical solutions with the elasticity solutions available in the literature; an excellent agreement is found. The layerwise beam model is then used to investigate the influence of transverse cracks on material properties and the response in cross-ply laminates using a multiscale approach. The multiscale analysis consists of numerical simulations at two different length scales. In the first scale, a mesoscale, a systematic procedure to quantify the stiffness reduction in the cracked ply is proposed exploiting the laminate theory. In the second scale, a macroscale, continuum damage mechanics approach is used to compute homogenized material properties for a unit cell, and the effective material properties of the cracked ply are extracted by the laminate theory. In the macroscale analysis, a beam structure under a bending load is simulated using the homogenized material properties in the layerwise finite element beam model. The stress redistribution in the beam according to the multiplication of transverse cracks is taken into account and a prediction of sequential matrix cracking is presented.

Keywords: Laminated composite beam; Finite element analysis; Layerwise theory; Nonlinear strain field; Transverse cracking; Multiscale analysis; Continuum damage mechanics

1 INTRODUCTION

DAMAGE in composite laminates subjected to various load conditions is of great interest in the design of composite structures. Most of the previous studies have only considered damage in composite laminates subjected to in-plane loads. Krajcinovic [1] proposed an analytical formulation to study the influence of distributed damage in composite laminates under pure bending loads. Echaani et al. [2] conducted a three-point-bending experiment to observe the progression of cracks in the composite laminate and suggested a criteria to predict a failure of the material. Murri and Guynn [3] conducted experiments to find the critical strain energy release rate for the delamination growth from matrix cracks under three different boundary conditions. Ogi et al. [4] made use of the shear lag model and classical beam theory to obtain the effective Young's modulus of the individual cracked ply. Similarly, the damaged material stiffness coefficients of the individual damaged ply were proposed by Boniface et al. [5]. To analyze the stress distribution of transversely cracked laminates under bending, Kuriakose and Talreja [6] attempted the variational solution, which is compared with the finite element solution. Most works on bending of composite laminates have been dedicated to the study of the effect of damage on the material stiffnesses, and only few works considered progressive damage and its effect on the load-carrying ability of the laminate. Also, these

* Corresponding author. Tel.: 979 862 2417; fax: 979 845 3081.
E-mail address: jnreddy@shakti.tamu.edu (J.N. Reddy).

studies have been limited to use of laminated beam theory with small deformations (i.e., the linear strain-displacement relations are used).

In this study, a multiscale approach is employed to predict the effective material properties and damage on the bending behavior of composite laminates. The layerwise theory of Reddy [7] is used to develop a finite element model in order to assess the stress responses of mesoscale and the macroscale model. The formulation includes the von Kármán type nonlinear strain field in order to accommodate the moderately large rotations under bending loads. The feasibility and accuracy of the layerwise beam model enable the multiscale analysis to be more realistic since the traditional laminate beam theories cannot capture the interlaminar stress fields accurately.

2 THEORETICAL FORMULATION

2.1 Equivalent single layer theories

A simple way to formulate a laminated beam is to rely on the conventional beam theories combined with the laminate theory. The material properties of each lamina can be taken care of by the classical laminate theory and the whole laminate can be dealt with as simple stacks of the laminate.

Two commonly used laminate beam models are the Euler-Bernoulli beam theory (EBT) and the Timoshenko beam theory (TBT). These two conventional beam theories are widely employed to give good results on analysis of relatively long and thin beams. In EBT, the displacement field is given

$$\begin{aligned} u(x,z) &= u_0(x,z) - z\frac{\partial w_0}{\partial x} \\ v(x,z) &= 0 \\ w(x,z) &= w_0(x,z) \end{aligned} \tag{1}$$

where (u_0, w_0) are the displacement components along the (x,z) coordinate directions, respectively, of a point on $z=0$ plane and the displacement fields in Eq. (1) are valid under the Euler-Bernoulli hypothesis. On the other hand, the displacement field in TBT is given by

$$\begin{aligned} u(x,z) &= u_0(x,z) + z\phi(x) \\ v(x,z) &= 0 \\ w(x,z) &= w_0(x,z) \end{aligned} \tag{2}$$

where $\phi(x)$ is an independent function of x and denotes rotation about the y axis. The Kirchhoff hypothesis is relaxed in TBT by removing the normality condition. In the course of developing an analytic model of the laminated beam, the kinematic representation of the deformation can be implemented in a finite element model with each layer's material properties. Although the material properties of each layer are taken into account, the equivalent single layer (ESL) theories (i.e., EBT and TBT) cannot accurately capture the interlaminar stresses, especially for the thick and short beams. On top of that, the ESL beam models often turn out to be improper for the damage analysis because the damage analysis requires a highly accurate assessment of localized stress fields [8].

2.2 Layerwise theory

In contrast to the equivalent single layer theories, both intralaminar and the interlaminar responses can be assessed with a high accuracy in the layerwise theory (LWT). The layerwise laminated beam model can be seen as a simplified version of the layerwise laminate plate model of Reddy [7]. In the original work of Reddy, the displacement-based theory of laminated plates has been treated. The main idea of Reddy's layerwise theory is that the three-dimensional elasticity theory can be reduced to a two-dimensional laminate theory by assuming the displacement field to vary as an explicit function of the thickness coordinate. Several studies ensued by making use of the layerwise plate theory of Reddy to analyze bending of beams [9, 10]. However, most of the works have dealt with beams based on the assumption of linearized strain fields. In the present work, a complete formulation of a layerwise beam model based on the nonlinear strain fields and the associated finite element model are developed.

2.3 Governing equations

Similar to the layerwise plate theory of Reddy [7, 8], the total displacement field of the laminated beam can be written as [9]

$$\begin{aligned} u(x,z) &= \sum_{I=1}^{N} U_I(x)\Phi^I(z) \\ v(x,z) &= 0 \\ w(x,z) &= \sum_{I=1}^{M} W_I(x)\Psi^I(z) \end{aligned} \tag{3}$$

where (U_I, W_I) denote the Ith nodal values of (u,w) while Φ^I and Ψ^I are the global interpolation functions (much like in the finite element method) for the longitudinal displacement and the transverse displacement through the thickness, respectively; N and M in Eq. (3) are the numbers of nodes through the thickness for the longitudinal displacement and the transverse displacement, respectively. In general, $\Phi^I \neq \Psi^I$ and $N \neq M$.

The von Kármán type nonlinear strains associated with the given displacement field are

$$\begin{aligned} \varepsilon_{xx} &= \frac{\partial u}{\partial x} + \frac{1}{2}\left(\frac{\partial w}{\partial x}\right)^2 \\ &= \sum_{I=1}^{N} \frac{dU_I(x)}{dx}\Phi^I(z) + \frac{1}{2}\left(\sum_{I=1}^{M} \frac{dW_I(x)}{dx}\Psi^I(z)\right)\left(\sum_{J=1}^{M} \frac{dW_J(x)}{dx}\Psi^J(z)\right) \\ \varepsilon_{zz} &= \frac{\partial w}{\partial z} = \sum_{I=1}^{M} W_I(x)\frac{d\Psi^I(z)}{dz} \\ \gamma_{xz} &= \frac{\partial w}{\partial x} + \frac{\partial u}{\partial z} = \sum_{I=1}^{M} \frac{dW_I(x)}{dx}\Psi^I(z) + \sum_{I=1}^{N} U_I(x)\frac{d\Phi^I(z)}{dx} \\ \varepsilon_{yy} &= \gamma_{xy} = \gamma_{yz} = 0 \end{aligned} \tag{4}$$

For the kth orthotropic lamina, the stresses can be obtained from the 3-D stress-strain relations

$$\begin{Bmatrix} \sigma_{xx} \\ \sigma_{yy} \\ \sigma_{zz} \\ \sigma_{yz} \\ \sigma_{xz} \\ \sigma_{xy} \end{Bmatrix}^{(k)} = \begin{bmatrix} \bar{C}_{11} & \bar{C}_{12} & \bar{C}_{13} & 0 & 0 & \bar{C}_{16} \\ \bar{C}_{21} & \bar{C}_{22} & \bar{C}_{23} & 0 & 0 & \bar{C}_{26} \\ \bar{C}_{31} & \bar{C}_{32} & \bar{C}_{33} & 0 & 0 & \bar{C}_{36} \\ 0 & 0 & 0 & \bar{C}_{44} & \bar{C}_{45} & 0 \\ 0 & 0 & 0 & \bar{C}_{54} & \bar{C}_{55} & 0 \\ \bar{C}_{61} & \bar{C}_{62} & \bar{C}_{63} & 0 & 0 & \bar{C}_{66} \end{bmatrix}^{(k)} \begin{Bmatrix} \varepsilon_{xx} \\ \varepsilon_{yy} \\ \varepsilon_{zz} \\ \gamma_{yz} \\ \gamma_{xz} \\ \gamma_{xy} \end{Bmatrix}^{(k)} \tag{5}$$

where $\bar{C}_{ij}^{(k)}$ are the transformed 3-D elastic coefficients [8]. The governing equations of the layerwise beam depicted in Fig. 1 are derived from the principle of virtual displacements [8, 11]

$$0 = \delta U + \delta V \tag{6}$$

where the virtual strain energy δU and the virtual work done by external forces δV are given by

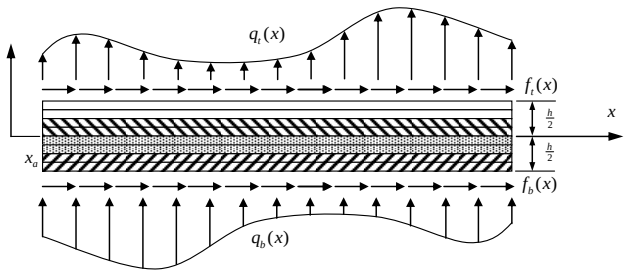

Fig. 1
A laminate beam model based on layerwise theory.

$$\delta U = \int_{x_a}^{x_b} \int_{-\frac{h}{2}}^{\frac{h}{2}} \sigma_{xx}\delta\varepsilon_{xx} + \sigma_{zz}\delta\varepsilon_{zz} + \sigma_{xz}\delta\gamma_{xz} \; dzdx \tag{7a}$$

$$\delta V = -\int_{x_a}^{x_b} f_b(x)\delta u(x,-\tfrac{h}{2}) + f_t(x)\delta u(x,\tfrac{h}{2}) \; dx - \int_{x_a}^{x_b} q_b(x)\delta w(x,-\tfrac{h}{2}) + q_t(x)\delta w(x,\tfrac{h}{2}) \; dx \tag{7b}$$

Applying the stress-strain relations in Eq. (5) and displacement field Eq. (3) to (7a) and (7b), the virtual strain energy and the virtual work done by external forces can be described in terms of the nodal displacements as

$$\delta U = \int_{x_a}^{x_b} \sum_{I=1}^{N} \left(N_{xx}^{I} \frac{d\delta U_I}{dx} + Q_x^I \delta U_I \right) dx + \int_{x_a}^{x_b} \sum_{I=1}^{N} \left(\sum_{J=1}^{M} N_{xx}^{IJ} \frac{d\delta W_I}{dx} \frac{dW_J}{dx} + Q_z^I \delta W_I + \tilde{Q}_x^I \frac{d\delta W_I}{dx} \right) dx \tag{8a}$$

$$\delta V = -\int_{x_a}^{x_b} f_b \delta U_1 + f_t \delta U_N \; dx - \int_{x_a}^{x_b} q_b \delta W_1 + q_t \delta W_M \; dx \tag{8b}$$

where

$$\begin{aligned}
N_{xx}^{I} &= \sum_{J=1}^{N} A_{11}^{IJ} \frac{dU_J}{dx} + \frac{1}{2}\sum_{J=1}^{M}\sum_{K=1}^{M} B_{11}^{IJK} \frac{dW_J}{dx}\frac{dW_K}{dx} + \sum_{J=1}^{M} \tilde{A}_{13}^{IJ} W_J \\
N_{xx}^{IJ} &= \sum_{K=1}^{N} B_{11}^{KIJ} \frac{dU_K}{dx} + \frac{1}{2}\sum_{K=1}^{M}\sum_{L=1}^{M} D_{11}^{IJKL} \frac{dW_K}{dx}\frac{dW_L}{dx} + \sum_{K=1}^{M} \tilde{B}_{13}^{IJK} W_K \\
Q_x^I &= \sum_{J=1}^{M} \bar{B}_{55}^{IJ} \frac{dW_J}{dx} + \sum_{J=1}^{N} \bar{A}_{55}^{IJ} U_J \\
\tilde{Q}_x^I &= \sum_{J=1}^{M} \bar{D}_{55}^{IJ} \frac{dW_J}{dx} + \sum_{J=1}^{N} \bar{B}_{55}^{JI} U_J \\
Q_z^I &= \sum_{J=1}^{N} \tilde{A}_{31}^{JI} \frac{dU_J}{dx} + \frac{1}{2}\sum_{J=1}^{M}\sum_{K=1}^{M} \tilde{B}_{31}^{JKI} \frac{dW_J}{dx}\frac{dW_K}{dx} + \sum_{J=1}^{M} \hat{A}_{33}^{IJ} W_J
\end{aligned} \tag{9}$$

and

$$\begin{aligned}
A_{11}^{IJ} &= \sum_{k=1}^{Ne} \int_{z_k}^{z_{k+1}} C_{11}^{(k)} \Phi^I \Phi^J dz \\
\tilde{A}_{13}^{IJ} &= \tilde{A}_{31}^{IJ} = \sum_{k=1}^{Ne} \int_{z_k}^{z_{k+1}} \bar{C}_{13}^{(k)} \Phi^I \frac{d\Psi^J}{dz} dz
\end{aligned} \tag{10}$$

$$\bar{A}_{55}^{IJ} = \sum_{k=1}^{Ne} \int_{z_k}^{z_{k+1}} \bar{C}_{55}^{(k)} \frac{d\Phi^I}{dz} \frac{d\Phi^J}{dz} dz$$

$$\hat{A}_{33}^{IJ} = \sum_{k=1}^{Ne} \int_{z_k}^{z_{k+1}} \bar{C}_{33}^{(k)} \frac{d\Psi^I}{dz} \frac{d\Psi^J}{dz} dz$$

$$\bar{B}_{55}^{IJ} = \sum_{k=1}^{Ne} \int_{z_k}^{z_{k+1}} \bar{C}_{55}^{(k)} \frac{d\Phi^I}{dz} \Psi^J dz$$

$$\bar{D}_{55}^{IJ} = \sum_{k=1}^{Ne} \int_{z_k}^{z_{k+1}} \bar{C}_{55}^{(k)} \Psi^I \Psi^J dz$$

$$B_{11}^{IJK} = \sum_{k=1}^{Ne} \int_{z_k}^{z_{k+1}} \bar{C}_{11}^{(k)} \Phi^I \Psi^J \Psi^K dz$$

$$\tilde{B}_{13}^{IJK} = \tilde{B}_{31}^{IJK} = \sum_{k=1}^{Ne} \int_{z_k}^{z_{k+1}} \bar{C}_{13}^{(k)} \Psi^I \Psi^J \frac{d\Psi^K}{dz} dz$$

$$D_{11}^{IJKL} = \sum_{k=1}^{Ne} \int_{z_k}^{z_{k+1}} \bar{C}_{11}^{(k)} \Psi^I \Psi^J \Psi^K \Psi^L dz$$

Here *Ne* denotes the number of physical layers in the laminate and the superscripts are introduced to match the superscripts of approximation functions in the definition of the quantities.

2.4 Finite element model

The displacement field (3) is approximated by appropriate interpolation functions in order to derive the finite element model of a layerwise beam

$$U_I(x) = \sum_{j=1}^{p} U_I^j \varphi_j^{(1)}(x), \quad W_I(x) = \sum_{j=1}^{q} W_I^j \varphi_j^{(2)}(x) \tag{11}$$

where P and q are the number of nodes per 1-D element used to approximate the longitudinal and transverse deflections, respectively, and U_I^j and W_I^j are the displacement values at the jth node along the longitudinal (x) direction of Ith beam element. The interpolation functions, $\varphi_j^{(1)}$ and $\varphi_j^{(2)}$ are the 1-D Lagrangian polynomials with respect to the longitudinal and transverse deflections at the jth node of each beam element. Substituting the approximation (11) for U_I and W_I, and

$$\delta U_I = \varphi_i^{(1)}(x), \quad \delta W_I = \varphi_i^{(2)}(x) \tag{12}$$

into the energy expressions (8a) and (8b) yields the finite element equations

$$\sum_{j=1}^{p}\sum_{J=1}^{N} K_{ij}^{(11)IJ} U_J^j + \sum_{j=1}^{q}\sum_{J=1}^{M} K_{ij}^{(12)IJ} W_J^j = {}^1F_i^I \tag{13a}$$

$$(i = 1,2,\cdots,p \text{ and } I = 1,2,\cdots,N)$$

$$\sum_{j=1}^{p}\sum_{J=1}^{N} K_{ij}^{(21)IJ} U_J^j + \sum_{j=1}^{q}\sum_{J=1}^{M} K_{ij}^{(22)IJ} W_J^j = {}^2F_i^I \tag{13b}$$

$$(i = 1,2,\cdots,q \text{ and } I = 1,2,\cdots,M)$$

where

$$
\begin{aligned}
K_{ij}^{(11)IJ} &= \int_{x_a}^{x_b}\left(A_{11}^{IJ}\frac{d\varphi_i^{(1)}}{dx}\frac{d\varphi_j^{(1)}}{dx}+\bar{A}_{55}^{IJ}\varphi_i^{(1)}\varphi_j^{(1)}\right)dx\\
K_{ij}^{(12)IJ} &= \int_{x_a}^{x_b}\left[\frac{1}{2}\left(\sum_{K=1}^{M}B_{11}^{IJK}\frac{dW_K}{dx}\right)\frac{d\varphi_i^{(1)}}{dx}\frac{d\varphi_j^{(2)}}{dx}+\tilde{A}_{13}^{IJ}\frac{d\varphi_i^{(1)}}{dx}\varphi_j^{(2)}+\bar{B}_{55}^{IJ}\varphi_i^{(1)}\frac{d\varphi_j^{(2)}}{dx}\right]dx\\
K_{ij}^{(21)IJ} &= \int_{x_a}^{x_b}\left[\left(\sum_{K=1}^{M}B_{11}^{IKJ}\frac{dW_K}{dx}\right)\frac{d\varphi_i^{(2)}}{dx}\frac{d\varphi_j^{(1)}}{dx}+\tilde{A}_{31}^{JI}\varphi_i^{(2)}\frac{d\varphi_j^{(1)}}{dx}+\bar{B}_{55}^{JI}\frac{d\varphi_i^{(2)}}{dx}\varphi_j^{(1)}\right]dx\\
K_{ij}^{(22)IJ} &= \int_{x_a}^{x_b}\frac{1}{2}\left(\sum_{K=1}^{M}\sum_{L=1}^{M}D_{11}^{IJKL}\frac{dW_K}{dx}\frac{dW_L}{dx}\right)\frac{d\varphi_i^{(2)}}{dx}\frac{d\varphi_j^{(2)}}{dx}dx\\
&\quad+\int_{x_a}^{x_b}\left[\left(\sum_{K=1}^{M}\tilde{B}_{13}^{IKJ}\frac{dW_K}{dx}\right)\frac{d\varphi_i^{(2)}}{dx}\varphi_j^{(2)}+\frac{1}{2}\left(\sum_{K=1}^{M}\tilde{B}_{31}^{JKI}\frac{dW_K}{dx}\right)\varphi_i^{(2)}\frac{d\varphi_j^{(2)}}{dx}\right]dx\\
&\quad+\int_{x_a}^{x_b}\left[\hat{A}_{33}^{IJ}\varphi_i^{(2)}\varphi_j^{(2)}+\bar{D}_{55}^{IJ}\frac{d\varphi_i^{(2)}}{dx}\frac{d\varphi_j^{(2)}}{dx}\right]dx
\end{aligned}
\tag{14}
$$

and

$$
{}^1F_i^I=\begin{cases}\displaystyle\int_{x_a}^{x_b}f_b(x)\varphi_i^{(1)}dx & I=1\\ \displaystyle\int_{x_a}^{x_b}f_t(x)\varphi_i^{(1)}dx & I=N\\ 0 & I=2,3,\cdots,N-1\end{cases}
\tag{15a}
$$

$$
{}^2F_i^I=\begin{cases}\displaystyle\int_{x_a}^{x_b}q_b(x)\varphi_i^{(2)}dx & I=1\\ \displaystyle\int_{x_a}^{x_b}q_t(x)\varphi_i^{(2)}dx & I=M\\ 0 & I=2,3,\cdots,M-1\end{cases}
\tag{15b}
$$

Note that the coefficient matrices $[K^{(12)}]$, $[K^{(21)}]$ and $[K^{(22)}]$ contain nonlinearity in such a way that they are functions of the unknown $W(x)$; also note that the finite element stiffness matrix is unsymmetric because $[K^{(12)}]^{\mathrm{T}}\neq[K^{(21)}]$ for the nonlinear case [12]. The Eqs. (13a) through (15b) are used to compute the nonlinear responses based on the direct iteration (linearization) or Newton-Raphson scheme. The direct iteration converges if the nonlinearity is not very prominent but it tends to diverge if the nonlinearity is severe. Divergence is more likely for hardening type nonlinearity [12]. The Newton-Raphson iterative method is employed to cover hardening types of nonlinear problems. The Newton-Raphson method makes use of the residual vector of the finite element Eqs. (13a), (13b) and its Taylor's series expansion about the solution from the previous iteration. Here the details of the Newton-Raphson method are omitted and, instead, the components of the tangent matrix [12] for the nonlinear layerwise beam model are listed as follows

$$
\begin{aligned}
T_{ij}^{(11)IJ} &= \int_{x_a}^{x_b} \left(A_{11}^{IJ} \frac{d\varphi_i^{(1)}}{dx} \frac{d\varphi_j^{(1)}}{dx} + \bar{A}_{55}^{IJ} \varphi_i^{(1)} \varphi_j^{(1)} \right) dx \\
T_{ij}^{(12)IJ} &= \int_{x_a}^{x_b} \left[\left(\sum_{K=1}^{M} B_{11}^{IJK} \frac{dW_K}{dx} \right) \frac{d\varphi_i^{(1)}}{dx} \frac{d\varphi_j^{(2)}}{dx} + \tilde{A}_{13}^{IJ} \frac{d\varphi_i^{(1)}}{dx} \varphi_j^{(2)} + \bar{B}_{55}^{IJ} \varphi_i^{(1)} \frac{d\varphi_j^{(2)}}{dx} \right] dx \\
T_{ij}^{(21)IJ} &= \int_{x_a}^{x_b} \left[\left(\sum_{K=1}^{M} B_{11}^{IKJ} \frac{dW_K}{dx} \right) \frac{d\varphi_i^{(2)}}{dx} \frac{d\varphi_j^{(1)}}{dx} + \tilde{A}_{31}^{JI} \varphi_i^{(2)} \frac{d\varphi_j^{(1)}}{dx} + \bar{B}_{55}^{JI} \frac{d\varphi_i^{(2)}}{dx} \varphi_j^{(1)} \right] dx \\
T_{ij}^{(22)IJ} &= \int_{x_a}^{x_b} \left(\sum_{K=1}^{N} B_{11}^{IJK} \frac{dU_K}{dx} \right) \frac{d\varphi_i^{(2)}}{dx} \frac{d\varphi_j^{(2)}}{dx} dx \\
&\quad + \int_{x_a}^{x_b} \frac{3}{2} \left(\sum_{K=1}^{M} \sum_{L=1}^{M} D_{11}^{IJKL} \frac{dW_K}{dx} \frac{dW_L}{dx} \right) \frac{d\varphi_i^{(2)}}{dx} \frac{d\varphi_j^{(2)}}{dx} dx \\
&\quad + \int_{x_a}^{x_b} \left[\left(\sum_{K=1}^{M} \tilde{B}_{13}^{IJK} W_K \right) \frac{d\varphi_i^{(2)}}{dx} \frac{d\varphi_j^{(2)}}{dx} + \left(\sum_{K=1}^{M} \tilde{B}_{31}^{JKI} \frac{dW_K}{dx} \right) \varphi_i^{(2)} \frac{d\varphi_j^{(2)}}{dx} \right] dx \\
&\quad + \int_{x_a}^{x_b} \left[\left(\sum_{K=1}^{M} \tilde{B}_{13}^{IKJ} \frac{dW_K}{dx} \right) \frac{d\varphi_i^{(2)}}{dx} \varphi_j^{(2)} + \bar{A}_{33}^{IJ} \varphi_i^{(2)} \varphi_j^{(2)} + A_{55}^{IJ} \frac{d\varphi_i^{(2)}}{dx} \frac{d\varphi_j^{(2)}}{dx} \right] dx
\end{aligned}
\tag{16}
$$

It is clear that unlike the unsymmetric coefficient matrix in the direct iteration method, the tangent stiffness matrix is symmetric even for the nonlinear case.

2.5 Numerical example

To demonstrate the accuracy of LWT, a simply supported laminated beam with [0/90/0] lay-up and subjected to the sinusoidally distributed transverse load is considered. Since an exact elasticity solution based on the linear strain fields is available for this example problem [13], the solutions from the linear finite element models based on all three different theories can be compared. One-half of the simply supported laminated beam is modeled using LWT, EBT, and TBT imposing the symmetry condition of rotation being zero at the midspan (x=L/2) of the beam. The meshes in the vicinity of the boundaries are gradually refined so that the Gauss points at which the computed stresses are close enough to the end points. Also, the number and the length of the elements of LWT, EBT and TBT are chosen in such a way that the Gauss points are same at which the stress is computed. A total 16 Lagrange quadratic beam elements are used for LWT and TBT while 32 Hermite cubic beam elements are used for EBT. As for the approximation of the displacement fields through the thickness in the model of LWT, two numerical layers per each physical layer are modeled using Lagrange quadratic interpolation functions for Φ^I and Ψ^I in Eq. (3). Note that the finite element models based on ESL theories are incapable of representing the layerwise kinematics of the laminated beam through the thickness (i.e., beam height).

The material properties of the unidirectional fibrous graphite/epoxy composite are taken as (see Pagano [13])

$$
\begin{aligned}
&E_1 = 25\times10^6 \text{ psi} \qquad && E_2 = E_3 = 1\times10^6 \text{ psi} \\
&G_{12} = G_{13} = 0.5\times10^6 \text{ psi} \qquad && G_{23} = 0.2\times10^6 \text{ psi} \\
&\nu_{12} = \nu_{13} = \nu_{23} = 0.25 .
\end{aligned}
$$

Fig. 2(a) shows the non-dimensional transverse deflections versus the length-to-thickness ratio and 2(b) displays the ratio of transverse deflections of each beam theory to the exact solutions.

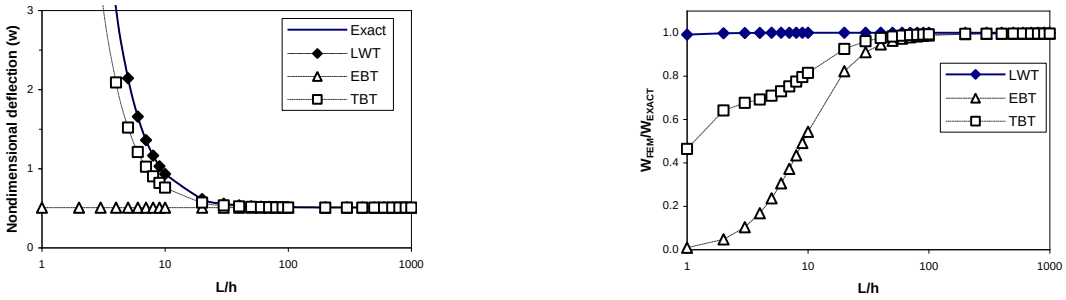

(a) (b)

Fig 2
Normalized transverse deflections of simply supported [0/90/0] laminate beams subjected to sinusoidally distributed transverse load; (a): $\bar{w} = w(L/2, h/2)E_2h^3/q_0L^4$, (b): w_{FEM}/w_{Exact} at (L/2, h/2).

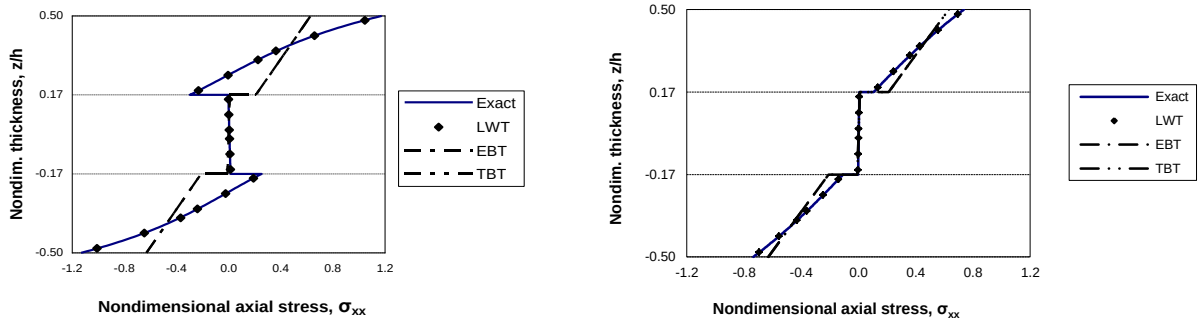

(a) (b)

Fig. 3
Nondimensional axial stress $\bar{\sigma}_{xx} = \sigma_{xx}(L/2, z)h^2/q_0L^2$ distribution through the thickness of simply supported [0/90/0] laminate beams subjected to sinusoidally distributed transverse load; (a): L/h=4, (b): L/h=10.

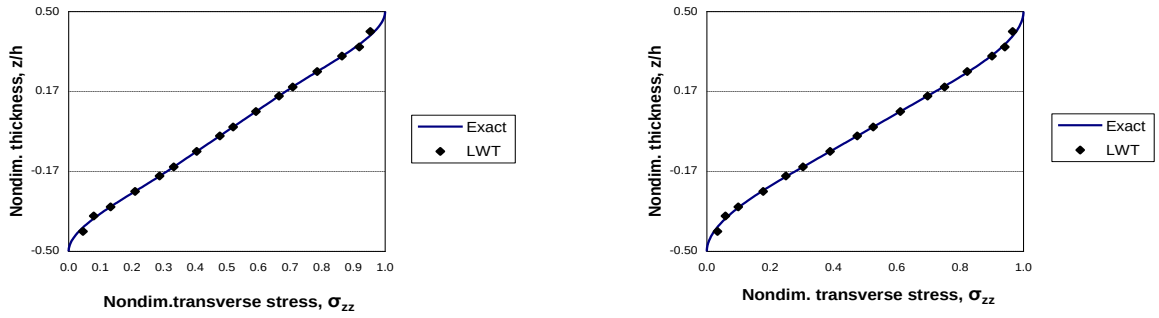

(a) (b)

Fig. 4
Nondimensional transverse stress $\bar{\sigma}_{zz} = \sigma_{zz}(L/2, z)1/q_0$ distribution through the thickness of simply supported [0/90/0] laminate beams subjected to sinusoidally distributed transverse load; (a): L/h=4, (b): L/h=10.

As seen in the figure, the LWT solution is in excellent agreement with the exact solutions in the range of length-to-thickness ratios considered. For the thick beams, namely, when the length-to-thickness ratio of the laminated beam is small, the ESL solutions are underestimated values compared to the LWT solutions. Especially, the EBT presents a poorer solution than the TBT does. However, as the beam gets thinner and longer, or as the length-to-thickness ratio increases, both the ESL solutions and the LWT solutions converge to the same solution.

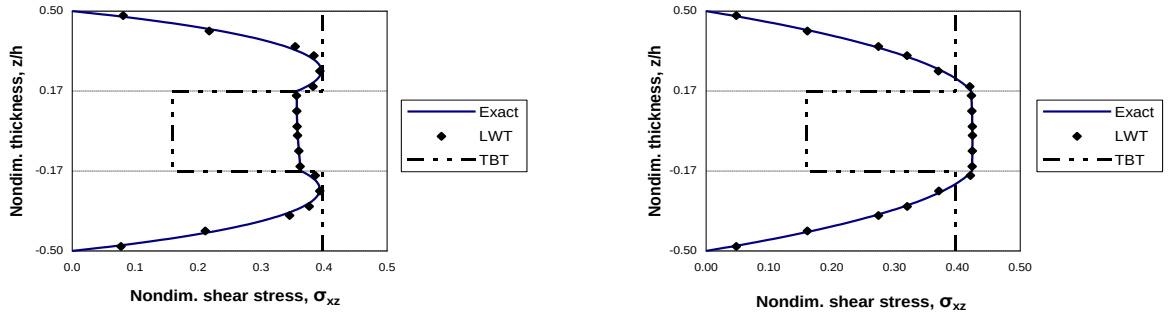

(a) (b)

Fig. 5

Nondimensional shear stress $\bar{\sigma}_{xz} = \sigma_{xz}(0,z)h / q_0 L$ distribution through the thickness of simply supported [0/90/0] laminate beams subjected to sinusoidally distributed transverse load; (a): L/h=4, (b): L/h=10.

The stresses through the thickness of the beams are shown in Fig. 3 through Fig. 5 for the linear case. The stresses are obtained at the reduced Gauss points closest to the position where each stress component reaches a maximum value.All the stresses obtained from the finite element models using LWT show very close agreement with the exact elasticity solutions whereas the ESL solutions considerably deviate from the exact elasticity solutions for the thick beam (L/h=4). It is noted that the transverse stress σ_{zz} is not available for the ESL beams and even the shear stress σ_{xz} cannot be obtained from the EBT due to the kinematic assumption of the theory. In contrast to the limitation of the ESL beams, the finite element model derived using the LWT is capable of yielding all three in-plane stresses as well as the deflection of the laminated beam with an excellent accuracy.

3 MODELLING OF TRANSVERSE CRACKS IN LAMINATE BEAMS

The continuum damage mechanics (CDM) has been studied profoundly and refined by a number of researchers [14, 15] since Kachanov [16] introduced its concept. Talreja [17, 18] is credited for applying the CDM theory systematically to a problem. In the CDM model of Talreja, the material coefficients are described at the level of laminated structure, that is, a macro scale. Hence, the characteristics of each ply are smeared out in the macro scale system, and the stiffness change in the individual ply of laminate structures cannot be specified. To overcome this shortcoming, Thionnet and Renard [19] applied Talreja's model to the ply level by using the classic laminate theory for the transverse cracks in cross-plies. Similarly, the damaged material stiffness coefficients of the individual damaged ply were proposed by Boniface et al. [5]. In addition to those, Li et al. [20] employed the strain energy equivalence to obtain the material stiffness coefficients of the individual damaged ply. The view that the transverse cracks in the laminate structure are a local phenomenon has been justified by the experimental observations and the results of the numerical computation [19]. In the current section, the transverse cracks in laminated beams are treated as a localized damage in the cracked ply, and a numerical computation is adopted to determine the damaged ply's homogenized material stiffness. A typical unit cell of the damaged laminate is taken from one transverse crack to the next under the assumption of uniform distance between the adjacent cracks.

3.1 Stiffness reduction scheme in mesoscale

One of the main difficulties of using Talreja's model is that the material constants used to evaluate the damage effects are determined by experimental data, and typically, the material constant associated with the change in the shear modulus cannot be determined due to large uncertainty in the measurement [21]. To construct a complete constitutive equation of the damaged material, Thionnet and Renard [19] evoked the conventional laminate plate theory in which the resultant homogenized material stiffness coefficients of the laminate are described as the superposition form of the material stiffnesses of the plies. In their work, the components of the homogenized material stiffness coefficients of the cracked ply have been derived on the cross-ply laminate. However, layers with any angle θ in the $[0_m / \theta_n]$ configurations are applicable to determine homogenized material stiffness coefficients of the cracked θ° ply in the laminate. Thus,

$$C_{11}^{D}=\frac{C_{22}^{H}-r^{0}C_{22}^{0}-r^{\theta}C_{22}^{\theta}}{r^{c}}$$
$$C_{12}^{D}=\frac{C_{12}^{H}-r^{0}C_{12}^{0}-r^{\theta}C_{12}^{\theta}}{r^{c}}$$
$$C_{22}^{D}=\frac{C_{11}^{H}-r^{0}C_{11}^{0}-r^{\theta}C_{11}^{\theta}}{r^{c}}$$
$$C_{66}^{D}=\frac{C_{66}^{H}-r^{0}C_{66}^{0}-r^{\theta}C_{66}^{\theta}}{r^{c}} \tag{17}$$

where the superscripts D, H, 0 and θ refer to the cracked ply, the total homogenized laminate, 0 degree and 90-degree ply, respectively (see Fig. 6). Also, the thickness ratio of each layer to the total laminate thickness is defined by

$$r^{D}=\frac{t^{D}}{h},\quad r^{0}=\frac{t^{0}}{h},\quad r^{\theta}=\frac{t^{\theta}}{h} \tag{18}$$

Here, a scalar damage variable is introduced to represent the damage state at a certain moment during the process of multiplication of the number of cracks, and it is defined using the geometry of Fig. 6(a) as

$$\boldsymbol{D}=\frac{t^{\theta}}{l} \tag{19}$$

where l is the length of the unit cell of the damaged laminate. The scalar damage variable $\boldsymbol{D}$ is often referred to as the normalized crack density. The normalized crack density will be an appropriate measure of the damage if the homogenized material stiffness coefficients of the damaged laminate vary with the change of $\boldsymbol{D}$. The total homogenized constitutive equation for the unit cell of a laminate beam that includes the cracked plies can be written as

$$\begin{Bmatrix}\sigma_1\\ \sigma_2\\ \sigma_6\end{Bmatrix}=\begin{bmatrix}C_{11}^{H} & C_{12}^{H} & 0\\ C_{12}^{H} & C_{22}^{H} & 0\\ 0 & 0 & C_{66}^{H}\end{bmatrix}\begin{Bmatrix}\varepsilon_1\\ \varepsilon_2\\ \varepsilon_6\end{Bmatrix} \tag{20}$$

If the homogenized material stiffness coefficients of the damaged laminate C_{ij}^{H} are known, the homogenized material stiffness coefficients of the cracked ply for a given damage state $\boldsymbol{D}$ are determined from Eq. (19). Yet, C_{ij}^{H} are the unknowns and should be determined by a proper numerical simulation.

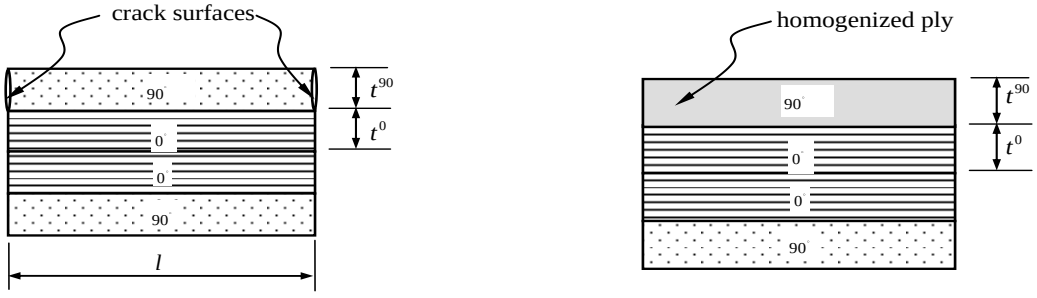

Fig. 6
Multiscale finite element model of $[90/0]_s$ laminate beam; (a): mesoscale model including cracks, (b): homogenized macroscale model.

In order to identify C_{ij}^{H}, the following four boundary conditions are imposed to the model shown in Fig. 6(a) for one value of the damage variable $\boldsymbol{D}$

$$\begin{aligned} &i)\ \ \varepsilon_1 = \varepsilon_{1c}\ \ ,\ \ \varepsilon_2 = 0 \\ &ii)\ \ \varepsilon_1 = \varepsilon_{1c}\ \ ,\ \ \varepsilon_2 = \varepsilon_{2c} \\ &iii)\ \ \varepsilon_2 = \varepsilon_{2c} \\ &iv)\ \ \varepsilon_6 = \varepsilon_{6c} \end{aligned} \tag{21}$$

where ε_{ic} represent arbitrary constants. Since the model (a) of Fig. 6 contains physical discontinuities inside the 90° ply, the strains and the stresses obtained from this model are not uniform. Hence, the strains and the stresses should be homogenized so that they can represent the equivalent values of homogenized material of the model (b). Using the homogenized strains and stresses computed from the unit cell model, the total homogenized material stiffness coefficients are given as

$$\begin{aligned} &i)\ \ C_{11}^{H} = \frac{\sigma_1}{\varepsilon_{1c}} \\ &ii)\ \ C_{12}^{H} = \frac{\sigma_1 - C_{11}^{H}\varepsilon_{1c}}{\varepsilon_{2c}} \\ &iii)\ \ C_{22}^{H} = \frac{\sigma_2}{\varepsilon_{2c}} \\ &iv)\ \ C_{66}^{H} = \frac{\sigma_6}{\varepsilon_{6c}} \end{aligned} \tag{22}$$

Substituting C_{ij}^{H} into (17a)-(17d) yields the homogenized material stiffness coefficients of the cracked ply. Additionally, the effective elastic moduli and Poisson's ratio of the cracked material can be extracted from the homogenized material stiffness coefficients of the associated ply as

$$\begin{aligned} E_1^D &= \frac{C_{11}^D C_{22}^D - (C_{12}^D)^2}{C_{22}^D} \\ E_2^D &= \frac{C_{11}^D C_{22}^D - (C_{12}^D)^2}{C_{11}^D} \\ G_{12}^D &= C_{66}^D \\ \nu_{12}^D &= \frac{C_{12}^D}{C_{22}^D} \end{aligned} \tag{23}$$

where the superscript *D* denotes the damaged ply and the subscripts refer to the material direction of the transformed composite layer.

3.2 Damage implementation on bending beam in macroscale

Once the relation between the normalized crack density and the material stiffness coefficients is obtained, the homogenized material stiffness coefficients of the cracked ply for a given damage state can be used for the damaged beam bending analysis. Identifying the stiffness reduction of the cracked ply enables the effect of transverse cracks to be included in the bending analysis of the laminated composite beam. An assumption is made to simplify the problem in the macroscale beam bending analysis: a beam element that reaches a critical strain value is assumed to be fully cracked over the entire element with a certain normalized crack density *D*. Therefore, the material properties

of the element showing the critical strain will be replaced by the homogenized values of the cracked ply which has been prepared in the mesoscale analysis.

4 NUMERICAL RESULTS AND DISCUSSION

A finite element model composed of plane elastic elements has been used to identify C_{ij}^H in [5, 19]. In the present study, the layerwise laminated beam model will be applied by taking advantage of the excellent accuracy of the solutions from LWT, as shown in the previous section. As demonstrated in the previous section, the layerwise laminated beam model is suitable for a mesoscale unit cell model with a small length-to-thickness ratio as well as the macroscale beam structure with a large length-to-thickness ratio.

Two finite element models using the layerwise laminate beam theory are depicted in Fig. 6. The model (a) of Fig. 6 is the numerical unit cell in the mesoscale and the model (b) of Fig. 6 is the homogenized laminate beam in the macroscale which will be utilized to analyze the bending behavior of the damaged beam. Naturally, two steps of numerical simulations are carried out according to the view of multiscale approach. At the first step of numerical simulation, a set of boundary conditions in Eq. (21) are imposed on the mesoscale unit cell model (a) of Fig. 6 to compute the stresses and eventually C_{ij}^H are determined. Once C_{ij}^H are known, the effective reduced material stiffness coefficients of the cracked ply are computed from Eq. (17a)-(17d). The second numerical computation step to analyze the bending behavior of the damaged beam is performed with the macroscale beam model (b) of Fig. 6 by replacing the material properties of the cracked plies with the homogenized values C_{ij}^D that are given in the first numerical simulation step.

4.1 Mesoscale analysis to identify material stiffness coefficients

The reduced material stiffness coefficients of a unit cell are computed for the same graphite/epoxy composite as chosen in the previous section but the laminate consists of $[90/0]_s$ lay-up. The half part of the unit cell is modeled with 8 quadratic beam elements using symmetric boundary conditions and each physical layer of the unit cell is interpolated by two quadratic Lagrange interpolation functions through the thickness. The lengths of the beam elements are gradually refined in the region which is close to the crack. Following the procedure explained with Eqs. (18) through (20), the homogenized material stiffness coefficients of the total laminate for the same laminate configuration is obtained and plotted in Fig. 7. It is noted in this figure that the ratio of the homogenized material stiffness coefficient to the virgin material stiffness coefficient of the total laminate gets smaller as the crack density is larger. The homogenized material stiffness coefficients of the cracked (90°) ply are computed by employing Eq. (16) from the homogenized material stiffness coefficients of the total laminate. Fig. 8 displays the decrease of material stiffness coefficients in the cracked ply with increasing the crack density. Note that the material direction of the 90° ply is marked in the graph so that C_{22}^D indicates the stiffness coefficient in the direction that is parallel to the fiber direction of the 0° ply. The effective engineering constants, such as Young's moduli (E_1^D, E_2^D), shear modulus (G_{12}^D), and Poisson's ratio (ν_{12}^D) of the cracked ply are shown in Fig. 9. It should be noted that the effective Young's modulus in the axial direction E_1^D of the 90° ply changes very little whereas the modulus in the transverse direction E_2^D is reduced drastically as the crack density increases. This result matches the observation reported in other literature that the presence of transverse cracks does not affect the effective Young's modulus along the fibers in the cracked lamina [20].

4.2 Macroscale analysis on damaged beam bending

Having the effective elastic moduli and Poisson's ratio of the cracked lamina facilitates the analysis on the bending behavior of transversely cracked laminate beams. Here, the $[90/0]_s$ cross-ply laminated beam is considered for the macroscale model and the effect of cracks in the individual lamina is treated as the effective material properties in the cracked lamina. Again, the laminated beam is modeled with the finite elements developed from LWT.

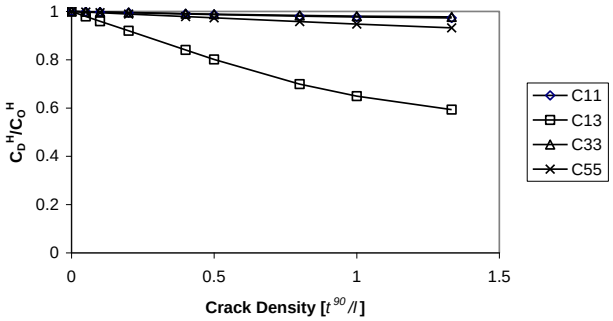

Fig. 7
Homogenized material stiffness coefficients of the total $[90/0]_s$ laminate.

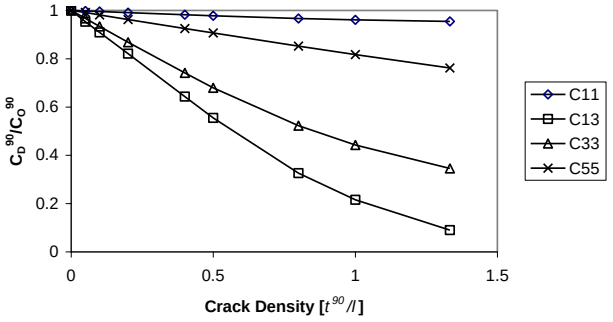

Fig. 8
Homogenized material stiffness coefficients of the cracked (90°) ply in $[90/0]_s$ laminate.

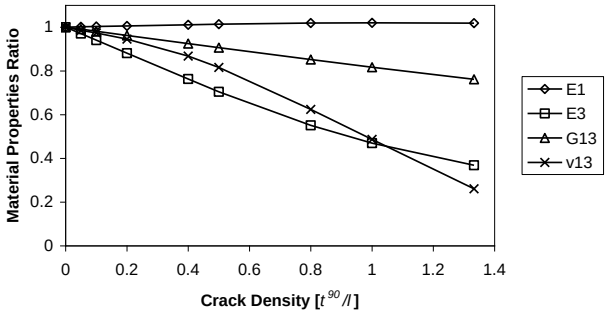

Fig. 9
Elastic moduli and Poisson's ratio reduction of the cracked ply in $[90/0]_s$ laminate.

Fig. 10 presents the configuration of the clamped-clamped boundary conditions and the load applied to the beam. The clamped boundary conditions at both ends of the beam are chosen so that the effect of nonlinearity in LWT can be prominent. Since the geometric symmetry of the beam is obvious, half of the full length of beam is modeled using symmetry boundary condition at $x=L/2$. Total 50 linear elements along the beam length (i.e. $L/2$=12.5 in) and 4 quadratic interpolation functions through the thickness (i.e. h=0.5 in) are used. The uniformly distributed load q_0 is applied and a constant load increment Δq is added at every load step until the uniformly distributed load reaches a final value of q_1 so that the composite laminate beam will carry increasingly varying loads and the transverse cracks will start forming in the 90° lamina. The critical load of forming the transverse cracks is determined by the critical axial normal stress at which the composite material fails. When the maximum stress in a 90° lamina becomes the critical stress, the material stiffness coefficients of the lamina in the associate finite element are replaced by the effective stiffness coefficients of the damaged material. The length of a single finite element is chosen such that the normalized crack density (t^{90}/l) equals one, which is assumed to be the characteristic damage state(CDS) [22]. That is, the number of cracks in the 90° lamina of the given length of the finite element is saturated, therefore, no more transverse cracks can form in the same lamina of the same element.

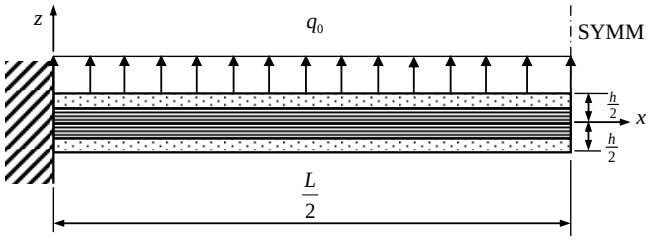

Fig. 10
Macroscale $[90/0]_s$ laminate beam model under a uniformly distributed load with clamped-clamped boundary conditions using geometric symmetry.

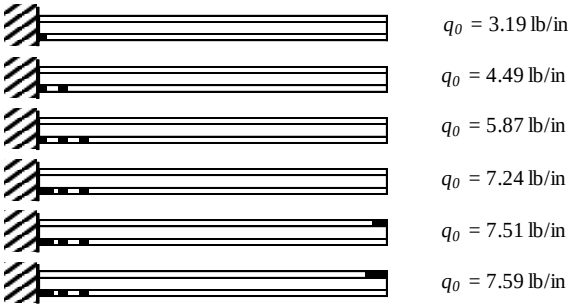

Fig. 11
Progress of transverse cracks in a clamped-clamped $[90/0]_s$ laminate beam.

The sequential progress of the cracked finite element according to increasing the load is depicted in Fig. 11 through a nonlinear analysis using the von Kármán type nonlinear strain. The area filled with black color represents the cracked lamina. The maximum stress in each lamina of the finite element is computed and compared with the critical stress at every load step. The material stiffness of the lamina showing the same value of the critical stress is replaced by the effective material stiffness which is obtained in the mesoscale analysis. Thus, every time the lamina meeting the criteria of transverse cracking is detected, the stress along the beam length is redistributed, and redistribution of the axial normal stress is shown for some increasing loads in Fig. 12. From Fig. 11, it is found that the first cracked element appears at the clamped end (i.e. x=0) and the cracked elements are multiplied from the clamped end to the midspan of the beam. And then, the cracks near the midspan of the beam start developing and they progressed toward the clamped end. The maximum transverse deflection at the top surface of the midspan of the beam is plotted at each load step in Fig. 13. Fig. 14 presents deformed shapes of the laminate beam under bending when the load q_0=20 lb/in, where many elements in the model appear damaged. The damaged beam shows larger transverse deflections as expected. It can be also seen that the effect of transverse cracks in the 90° ply is more prominent for the linear beam than the nonlinear case. The axial normal stress σ_{xx} on the tensile surface is plotted in Fig. 15 and Fig. 16. As shown in Fig. 12, the bottom 90° layer near the clamped end is expected to be damaged due to the tensile stress under bending and the top 90° layer near the midspan of the beam is expected to be cracked later. Thus, the stresses are computed at the nearest Gauss point to the bottom surface (i.e. z=-h/2) of the clamped end (i.e. x=0) in Fig. 15 and the top surface (z=h/2) of the center of beam (i.e. x=L/2) in Fig. 16. In the figure, the capacity to carry the axial load in the damaged lamina can be seen and the transverse cracking damage seems to diminish it radically. According to the present numerical result, the initial crack at the clamped end is formed at a relatively low applied load (i.e. q_0=3.16 for linear beam and q_0=3.19 for nonlinear beam) and the linear and the nonlinear beam show almost same stress change at this moment because the crack starts forming before the nonlinearity appears in the beam (see Fig. 13). However, in Fig. 16, the nonlinear curve is found to diverge from the linear curve around the applied load q_0=5 which is before the initial transverse crack forms at the midspan of the beam. In other words, the transverse cracking at the midspan of the beam starts after the nonlinearity develops in the beam. Therefore, the nonlinear analysis appears to be required to predict multiplication of the transverse cracking for this case. On the other hand, it can be appreciated from Fig. 16 that the nonlinear beam sustains a higher applied load before the cracks are formed at the center of the laminated beam. Another interesting finding is that the second stress drop is observed in Fig. 15 at the same applied load of forming cracks at the midspan of the beam. On the contrary, no stress drop is found in Fig. 16 when the clamped boundary end is damaged. Only one big stress drop is found commonly in the linear and the nonlinear beam when the midspan of the beam itself is damaged.

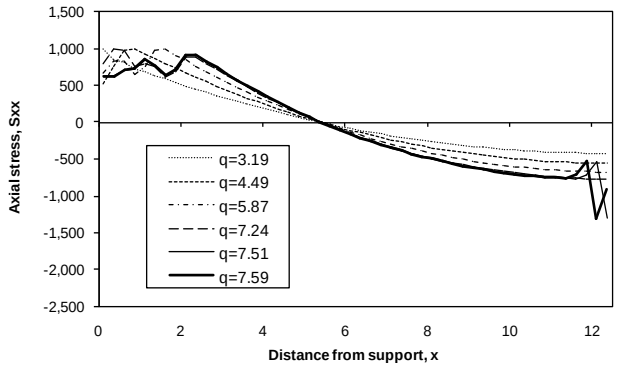

(a)

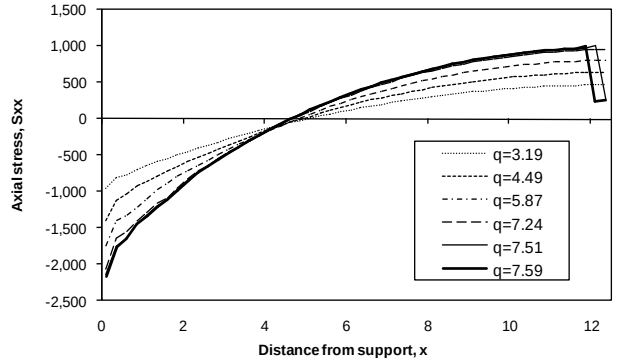

(b)

Fig. 12
Redistribution of the axial normal stress along the beam; (a): at the lower 90° lamina, $\sigma_{xx}(x,-h/2)$, (b): at the upper 90° lamina, $\sigma_{xx}(x,h/2)$.

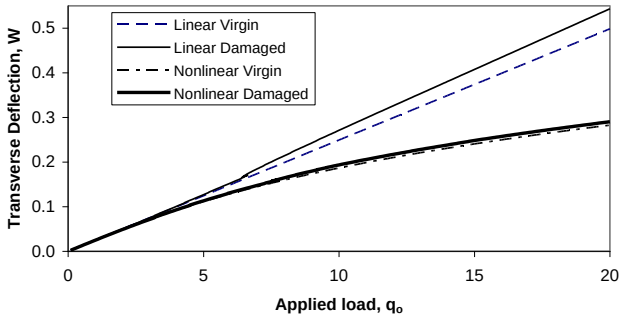

Fig. 13
Transverse deflection $w(L/2,h/2)$ versus the applied load of a clamped-clamped $[90/0]_s$ laminate beam.

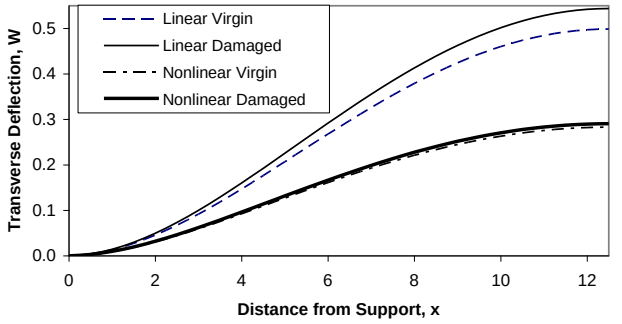

Fig. 14
Transverse deflection $w(x,h/2)$ under q_0=4 (lb/in) along the length of a clamped-clamped $[90/0]_s$ laminate beam.

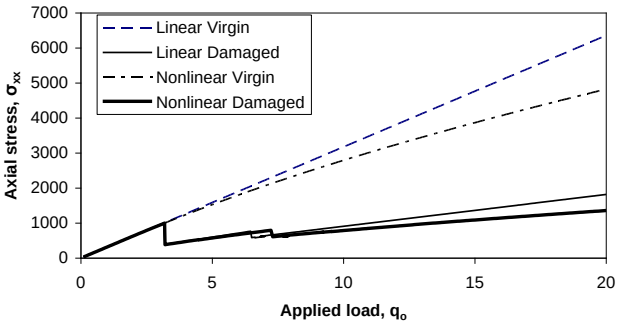

Fig. 15
Axial stress at the clamped end $\sigma_{xx}(0,-h/2)$ versus the applied load in a clamped-clamped $[90/0]_s$ laminate beam.

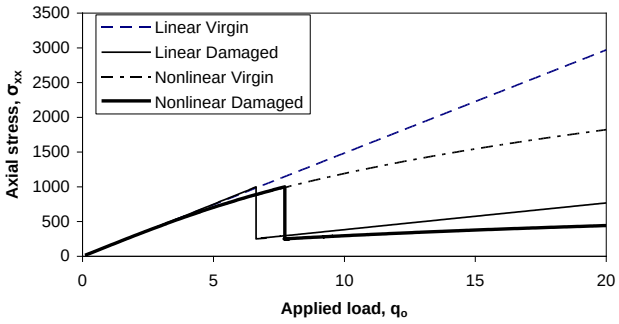

Fig. 16
Axial stress at the midspan of the beam $\sigma_{xx}(L/2,h/2)$ versus the applied load in a clamped-clamped $[90/0]_s$ laminate beam.

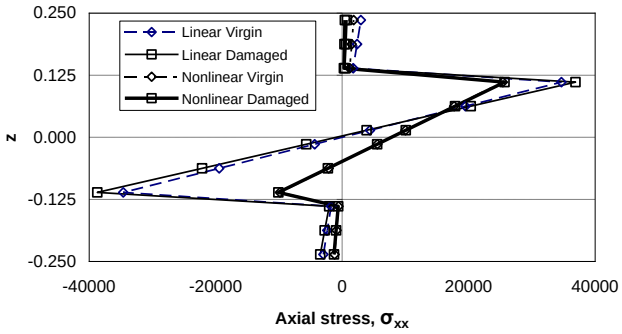

Fig. 17
Axial stress distribution $\sigma_{xx}(L/2,z)$ through the thickness of a clamped-clamped $[90/0]_s$ laminate beam.

One can draw a deduction from this observation that the damage around the clamped boundary region has little influence on the stress field of the midspan of the beam under a bending load. The stress distribution through the thickness of the laminate near the midspan of the beam under the applied load (q_0=20 lb/in) is displayed in Fig. 17 through Fig. 19. In Fig. 17, the axial normal stress is reduced through the thickness when the damage is considered in the laminate beam. The damaged 90° ply shows little capacity to carry the axial load. More importantly, the neutral axis, at which the axial normal stress $\sigma_{xx}=0$, is shifted from z=0 axis to the compressive side for the nonlinear beam case, whereas the linear beam shows a symmetric stress distribution about z=0 axis. Considering that the transverse cracking starts after the kinematic nonlinearity develops, the nonlinear beam model is suitable for this problem because its capability to capture the shift of neutral axis to the compressive side under a large deformation appears to give more practical solutions. Fig. 18 displays the transverse normal stress distribution through the thickness. The beam shows a large compressive stress in the 90° plies when the transverse cracking is taken into account while the transverse normal stress change in the core (i.e. 0° plies) of the laminate is not noticeable. The shear stress distribution through the thickness is shown in Fig. 19. A significant change of shear stress at the midspan of the beam is not found when the effect of transverse cracking is imposed in the clamped-clamped model. The nonlinear analysis shows the less shear stress through the thickness than the linear analysis result as expected.

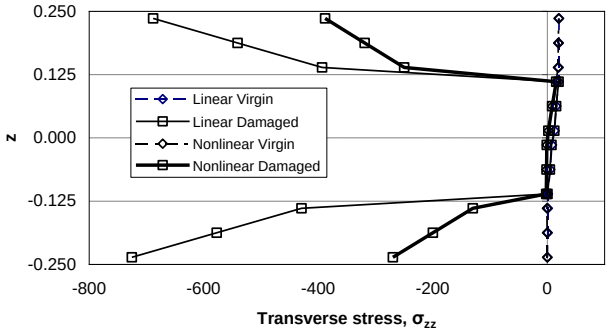

Fig. 18
Transverse stress distribution $\sigma_{zz}(L/2,z)$ through the thickness of a clamped-clamped $[90/0]_s$ laminate beam.

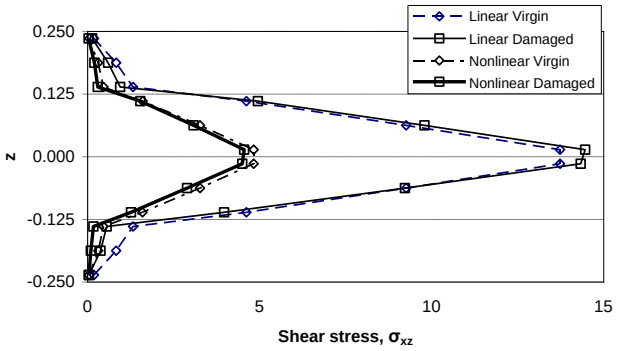

Fig. 19
Shear stress distribution $\sigma_{xz}(L/2,z)$ through the thickness of a clamped-clamped $[90/0]_s$ laminate beam.

5 CONCLUSIONS

A finite element model for the laminate beam based on von Kármán type nonlinear strain field and layerwise theory is developed. The finite element model of layerwise laminate beam provides accurate solutions showing an excellent agreement with the exact elasticity solutions in terms of stresses as well as deflections.
Using the multiscale analysis approach, two steps of numerical simulations can be carried out using LWT and the effort to construct a number of meshes can be minimized in the present multiscale damage analysis. The layerwise laminate beam model is used to analyze the unit cell of the transversely cracked laminate in mesoscale in order to determine the material properties of the damaged lamina. The analysis on the bending behavior of the transversely cracked laminate beam in macroscale can be performed by replacing the material properties obtained from the mesoscale model for the cracked ply. As a result, a prediction of the sequential transverse cracking in a laminated beam is demonstrated through a numerical example of the $[90/0]_s$ cross-ply laminated beam subjected to a bending load.

A laminated beam is analyzed under a distributed load with a clamped-clamped boundary condition using the nonlinear laminate beam model derived on LWT. It is found that the nonlinear beam model is inevitable for the study for transverse cracking, especially when the damage occurs under a large deformation so that the geometric nonlinearity develops before the material is damaged. Further, the feature of the largely deformed bending beam such as the shift of neutral axis can be captured by the nonlinear laminate beam model using LWT. For the clamped-clamped bending beam case, it is also found that the damage at the center of the bending beam affects redistribution of the stress at the clamped boundary end whereas the damage at the clamped boundary end does not disturb the stress at the midspan of the beam.

Acknowledgements

The research reported herein was carried out while the first author was supported by US Army Grant 45508-EG and Oscar S. Wyatt Endowed Chair.

REFERENCES

[1] Krajcinovic D., 1979, Distributed damage theory of beams in pure bending, *Journal of Applied Mechanics* **46**(3): 592-596.

[2] Echaani J., Trochu F., Pham X.T., Ouellet M., 1996, Theoretical and experimental investigation of failure and damage progression of graphite-epoxy composites in flexural bending test, *Journal of Reinforced Plastics and Composites* **15**(7): 740-755.

[3] Murri G.B., Guynn, E.G., 1988, Analysis of delamination growth from matrix cracks in laminates subjected to bending loads, *Composite Materials: Testing and Design*, ASTM Special Technical Publication **972**: 322-339.

[4] Ogi K., Smith P.A., 2002, Characterisation of Transverse Cracking in a Quasi-Isotropic GFRP Laminate under Flexural Loading, *Applied Composite Materials* **9**(2): 63-79.

[5] Boniface L., Ogin S.L., Smith P.A., 1991, Strain energy release rates and the fatigue growth of matrix cracks in model arrays in composite laminates, in: *Proceedings Mathematical and Physical Sciences* **432**(1886): 427-444.

[6] Kuriakose S., Talreja R., 2004, Variational solutions to stresses in cracked cross-ply laminates under bending, *International Journal of Solids and Structures* **41**: 2331-2347.

[7] Reddy J.N., 1987, A generalization of two-dimensional theories of laminated composite plates, *Communications in Applied Numerical Methods* **3**(3): 173-180.

[8] Reddy J.N., 2004, *Mechanics of Laminated Composite Plates and Shells - Theory and Analysis*, CRC Press, Boca Raton, FL.

[9] Robbins D.H., Reddy J.N., 1991, Analysis of piezoelectrically actuated beams using a layer-wise displacement theory, *Computers and Structures* **41**(2): 265-279.

[10] Rosca V.E., Poterasu V.F., Taranu N., Rosca B.G., 2002, Finite-element model for laminated beam-plates composite using layerwise displacement theory, *Engineering Transactions* **50**(3): 165-176.

[11] Reddy J.N., 2002, *Energy Principles and Variational Methods in Applied Mechanics*, John Wiley & Sons, Inc., Hoboken, New Jersey.

[12] Reddy J.N., 2004, *An Introduction to Nonlinear Finite Element Analysis*, Oxford University Press, New York.

[13] Pagano N.J., 1969, Exact solutions for composite laminates in cylindrical bending, *Journal of Composite Materials* **3**: 398-411.

[14] Krajcinovic D.K., 1984, Continuum damage mechanics, *Applied Mathematics Reviews* **37**(1): 1-6.

[15] Lemaitre J., 1984, How to use damage mechanics, *Nuclear Engineering and Design* **80**(2): 233-245.

[16] Kachanov L.M., 1958, Rupture time under creep conditions, *Izvestia Academii Nauk SSSR, Otdelenie tekhnicheskich, nauk*, **8**: 26-31.

[17] Talreja R., 1985, A continuum mechanics characterization of damage in composite materials, in: *Proceedings of Royal Society of London, Series A* **399**(1817): 195-216.

[18] Talreja R., 1985, Transverse cracking and stiffness reduction in composite laminates, *Journal of Composite Materials* **19**(4): 353-375.

[19] Thionnet A., Renard J., 1993, Meso-Macro approach to transverse cracking in laminated composites using Talreja's model, *Composites Engineering* **3**(9): 851-871.

[20] Li S., Reid R., Soden P.D., 1998, A continuum damage model for transverse matrix cracking in laminated fibre-reinforced composites, in: *Philosophical Transactions of the Royal Society London, Series A* **356**(1746): 2379-2412.

[21] Talreja R., 1990, Internal variable damage mechanics of composite materials, *Yielding Damage and Failure of Anisotropic Solids*, Mechanical Engineering Publications, London, 509-533.

[22] Reifsnider K.L., Masters J.E., 1978, Investigation of characteristic damage states in composite laminates, *ASME Paper*, 78WA/Aero-4: 1-10.